CIV Absorption From Galaxies in the Process of Formation

Martin G. Haehnelt[1], Matthias Steinmetz[1,4] & Michael Rauch[2,3]

mhaehnelt@mpa-garching.mpg.de, msteinmetz@mpa-garching.mpg.de, mr@astro.caltech.edu

Subject Headings: cosmology: theory, observation — galaxies: formation, evolution — intergalactic medium — quasars: absorption lines

1996, Astrophysical Journal Letters, 465, L95

Received: ______________; *Accepted:* ______________

Abstract

We investigate the heavy element QSO absorption systems caused by gas condensations at high redshift which evolve into galaxies at the present epoch. Artificial QSO spectra were generated for a variety of lines-of-sight through regions of the universe simulated with a hydrodynamics code. The CIV and HI absorption features in these spectra closely resemble observed CIV and HI absorption systems if [C/H] ~ -3 to -2 is assumed. CIV absorption complexes with multiple-component structure and velocity spreads up to $\sim 600\,\mathrm{km\,s^{-1}}$ are found. The broadest systems are caused by lines-of-sight passing through groups of protogalactic clumps aligned along filamentary structures expanding with the Hubble flow. Typical clumps have a radius of about $5-10\,\mathrm{kpc}$, a baryonic mass of $\sim 10^9\,\mathrm{M_\odot}$ and are surrounded by hot gas atmospheres with radius of about $30\,\mathrm{kpc}$. The temperature of a considerable fraction of the gas does not take the photoionization equilibrium value. This invalidates density and size estimates derived from thermal equilibrium models. Our model may be able to explain both high-ionization multi-component heavy-element absorbers and damped Lyα systems as groups of small protogalactic clumps.

[1]Max-Planck-Institut für Astrophysik, Karl-Schwarzschild-Straße 1, Garching, Germany

[2]Astronomy Dept., 105-24 California Institute of Technology, Pasadena 91125, USA

[3]Hubble Fellow

[4]present address: Dept. of Astronomy, UC Berkeley 94720, USA

1 Introduction

Heavy element absorption as seen in the spectra of distant quasi-stellar objects (QSOs) is commonly thought to be produced by metal-contaminated gas associated with galaxies. At low and intermediate redshift a connection of low-ionization metal absorption systems with observable galaxies is strongly indicated by successful searches for galaxies close to the absorption redshift (Bergeron 1986; Bergeron & Boissé 1991; Lanzetta et al. 1995; Steidel 1995).

However, such a close one-to-one correspondence between galaxy and absorption system need not be valid for higher-ionization (CIV) systems at higher redshifts (York 1988). Several features like the extended component structure of CIV selected absorption systems are equally difficult to understand in terms of a stationary cloudlet-in-halo model as in terms of absorption along lines-of-sight (LOS) through known types of local galaxy clusters (Pettini et al. 1983; Morris et al. 1986, Mo 1994). Instead, going back in time we should ultimately see the small-scale gas condensations from which instabilities and hierarchical clustering have build up present-day galaxies (Lake 1988, Steidel 1990).

Numerical simulations of the large-scale distribution of neutral hydrogen have recently lead to a major advance in the understanding of Lyα absorption systems (Cen et al. 1994; Petitjean, Mücket & Kates 1995; Hernquist et al. 1995). Here we investigate smaller scales in order to understand the nature of heavy element absorption systems. We have used a set of Smoothed-Particle-Hydrodynamics (SPH) simulations to model the detailed evolution of regions which by the present epoch contain one to three galaxies with halo circular velocities between 100 and 200 $\mathrm{km\,s^{-1}}$. We focus on the CIV absorption properties of these regions. Recent spectroscopic studies by Tytler et al. (1995) and Cowie et al. (1995) indicate that all baryonic matter at the relevant redshift could be contaminated with heavy elements to some degree. For simplicity we assume in the present paper a small homogeneously distributed fraction of metals.

In section 2 we describe the technical details of the SPH simulations and of our determination of the ionization state of carbon. Section 3 illustrates the characteristic features of CIV absorption in our simulations and in section 4 we discuss some implications.

2 The spatial distribution of neutral hydrogen and CIV

2.1 Simulating the gas distribution

The simulations were performed using GRAPESPH (Steinmetz 1996). The cosmological background model is a $\Omega = 1$, $H_0 = 50$ $\mathrm{km\,s^{-1}}$ $\mathrm{Mpc^{-1}}$ cold dark matter (CDM) cosmogony with a normalization of $\sigma_8 = 0.63$. The baryon fraction is $\Omega_b = 0.05$. The mass resolution is 5×10^6 $\mathrm{M_\odot}$ to 2×10^7 $\mathrm{M_\odot}$ for the gas. The gravitational softening is 1.25–2.5 kpc for the gas and a factor of two larger for the dark matter. The simulations cover a high resolution sphere with a radius of about 2–4 Mpc. The tidal field due to surrounding matter was taken into account using the multi-mass technique described in Navarro, Frenk, & White (1995). For the UV background we assume the redshift dependence given by Vedel, Hellsten & Sommer–Larsen (1994),

$$J(\nu) = 10^{-21} \left[1 + \left(\frac{5}{1+z}\right)^4\right]^{-1} \left(\frac{\nu}{\nu_H}\right)^{-\alpha} \mathrm{erg\,s^{-1}\,cm^{-2}\,Hz^{-1}\,str^{-1}}, \tag{1}$$

where ν_H is the frequency corresponding to the ionization energy of hydrogen (13.6 eV). For α a value of 1.5 was usually assumed.

2.2 The ionization state of the gas

We have used the photoionization code CLOUDY to calculate the ionization state of carbon (Ferland 1993). CLOUDY was used in its "Lyα absorber mode". The solid curves in Figure 1a show the column density ratio of CIV and neutral hydrogen for [C/H] $= -2$, a UV background given by equation (1) with $\alpha = 1.5$ and $z = 3$, and a fixed temperature as indicated on the plot. For the dashed curve the temperature was assumed to be determined by photoionization equilibrium. Figure 1b shows a typical scatter plot of density versus temperature of the SPH particles in our simulations. Around the peak of the equilibrium curve the temperature is generally larger than the equilibrium value due to compressional heating. Also seen is a modest deviation from the equilibrium curve towards smaller temperatures due to adiabatic cooling at the lowest densities.

3 Absorption spectra

3.1 General appearance of absorption features

In Figure 2 and 3 we show artificial spectra which were produced with a signal-to-noise of 50, an instrumental broadening of $8\,\mathrm{km\,s^{-1}}$, and a bin size of $2\,\mathrm{km\,s^{-1}}$ to match the spectral resolution obtainable with the HIRES spectrograph of the Keck telescope. A Voigt profile with optical depth and width corresponding to its temperature and column density was generated for each volume element in the box. The contributions from all such individual profiles to the optical depth in a given velocity bin where then co-added to produce the full spectrum. HI and CIV are overplotted in velocity space. For clarity we plot only the $\lambda1548$ line of the CIV doublet.

The spectra generally show a convincing resemblance both to the weak CIV absorption systems observed e.g. by Cowie et al. (1995) and others and the stronger variants seen in low-resolution CIV surveys (e.g. Sargent, Boksenberg & Steidel 1988). Figure 2 shows the HI and CIV absorption for a 5×5 mosaic of LOS around a filamentary structure at $z = 3$. The proper distance between the panels is 10 kpc. The LOS at the center penetrates about 5 to 7 different clumps (see also Figure 4b) producing a prominent clusters of CIV lines. The clustering pattern varies considerably over scales of 5 kpc. At a distance of about 30 kpc the CIV absorption has almost dropped below the detection threshold.

3.2 Velocity structure

In Figures 3a and 3b we present two different kinds of structures which we found to be responsible for prominent clusters of narrow CIV absorption lines. The four upper panels show the absorption, the density, the CIV and HI weighted temperatures, and the velocity profile along the LOS. The bottom panels contain CIV density contour maps. The contour plot and the density profile of Figure 3a shows that the LOS penetrates a single clump. The temperature is clearly enhanced above the ionization equilibrium temperature and the complicated temperature profile is responsible for the cluster of CIV lines. The object is obviously not dynamically relaxed. Figure 3b shows a LOS along a filamentary structure. The alignment of 5 to 7 well separated clumps none of which has a circular velocity larger than about $100\,\mathrm{km\,s^{-1}}$ is responsible for the prominent CIV cluster which extends over $500\,\mathrm{km\,s^{-1}}$. The broadest and most complex absorption features found in our simulations are produced by such an alignment of dense clumps along filaments.

3.3 Abundance determinations

Determining metal abundances from QSO absorption lines requires at least one pair of ionic species occupying the same spatial region and experiencing the same physical conditions. For low-column-density systems, however, there is often only the CIV/HI ratio available. As shown in Figure 1a, for the equilibrium case with temperatures of about 10^4 K there is a broad peak in the CIV/HI column-density ratio, log(CIV/HI) $\sim$ [C/H] which extends over two to three orders of magnitude in density. Cowie et al. (1995) therefore infer [C/H]$= -3$ to -2 from their measured CIV/HI column density ratios of about 10^{-3} to 10^{-2}. For our simulations we find that this assumption gives generally reasonable results. However, as shown in Figure 3d, for some LOS this reasoning can fail by a large margin. Despite the fact that [C/H]$= -2$, the CIV column density here is only a factor eight smaller than the HI column density. These rather rare LOS pass through the hot atmospheres of dense clumps with gas temperatures close to 3×10^5 K where the CIV/HI ratio reaches a maximum for collisionally ionized gas (see Figure 1a).

4 Discussion and Conclusions

We have demonstrated that LOS through regions of ongoing galaxy formation can produce CIV absorption complexes very similar to the ones actually observed. The individual CIV components are related to protogalactic condensations (PGC) with baryonic masses of about $10^9\,\mathrm{M_\odot}$ and radii of about $5 - 10\,$kpc.

The PGCs are in a variety of dynamical states. Velocity dispersions in the CIV absorption system of a few hundred km/s are often due to small-scale motions of bound objects, while larger velocities usually arise from the large-scale expansion of the universe and the fortuitous orientation of the LOS along an expanding filament. This interpretation avoids the difficulties associated with accounting for systems with velocity extent in excess of $500\,\mathrm{km\,s^{-1}}$ in terms of galaxy clusters or clouds orbiting in massive halos at these high redshifts (see also Pettini et al. 1983 and Morris et al. 1986).

If we choose a LOS through the very center of a PGC, the HI column density easily exceeds $10^{20}\,\mathrm{cm}^{-2}$. Thus our findings may also be relevant for an understanding of damped Lyα systems. The observed component structure of higher ions associated with damped Lyα systems is very similar to those of non-damped CIV systems. The main difference between CIV-'only' and damped Lyα systems could thus be one of impact parameter implying a possible unified picture in which both are caused by groups of PGCs. However, for a rigorous investigation of this question optical depth effects would have to be taken into account. Evidence for damped Lyα systems as small as the PGCs discussed here comes from observational work of of Møller & Warren (1995; Warren & Møller 1995; cf. Wolfe 1995) and theoretical work by Kauffmann (1995).

The complex component structures arises from density and temperature profiles which vary strongly along the LOS. The assumption that the temperature takes the photoionization equilibrium value, often made in photoionization models, will fail in such cases (see also Miralda-Escudé & Rees 1993). Even for a correctly determined density , the fraction of neutral hydrogen is then systematically overestimated (Haehnelt, Rauch & Steinmetz 1996). This can lead to severe underestimates of the cloud size along the LOS and might explain the very small CIV cloud sizes of $\sim$ 100 pc inferred by Cowie et al. (1995). Abundance determinations which assume the gas to be close to the photoionization equilibrium temperature should generally give acceptable abundances. Nevertheless, abundance determinations on the basis of CIV/HI column density ratios alone should be considered with some caution.

Although very idealized, a homogeneous metal contamination of the intergalactic medium with [C/H] ~ -2 leads to an astonishingly good representation of the observed CIV absorption. The appearance of the absorption line complexes is determined mainly by the temperature and ionization structure of the density maxima and by the large-scale dynamics of the PGC groups. Thus we expect that our results will not change much, if the metals are not homogeneously distributed.

We conclude that the gas physics and the mass scales included in our simulations of regions of ongoing galaxy formation are sufficient to recover the basic properties of observed CIV absorption systems.

5 Acknowledgments

We thank Martin Rees and Simon White for very helpful comments and Gary Ferland for making CLOUDY available to us. MR acknowledges instructive conversations with Bob Carswell, Len Cowie, Esther Hu, Palle Møller, Ray Weymann and Wal Sargent, and is grateful to NASA for support through grant HF-01075.01-94A from the Space Telescope Science Institute, which is operated by the Association of Universities for Research in Astronomy, Inc., under NASA contract NAS5-26555. Support by NATO grant CRG 950752 and the "Sonderforschungsbereich 375-95 für Astro-Teilchenphysik der Deutschen Forschungsgemeinschaft" is also gratefully acknowledged. MGH thanks Wal Sargent and Caltech for hospitality.

References

Bergeron J., 1986, A&A, 155, L8

Bergeron J., Boissé P., 1991, A&A, 243, 344

Cen R., Miralda-Escudé J., Ostriker J.P., Rauch M., 1994, ApJ, 437, L9

Cowie L.L., Songaila A., Kim T.-S., Hu E. 1995, AJ, 109, 1522

Donahue M., Shull J.M., 1991, ApJ, 383, 511

Ferland G.J., 1993, University of Kentucky Department of Physics and Astronomy Internal Report

Haehnelt, M.G., Steinmetz, M., Rauch, M. in prep.

Kauffmann G.A.M., 1996, to appear in *"Cold Gas at High Redshift"*, eds. Bremer M., Van der Werf P., Carilli C.

Hernquist L., Katz N., Weinberg D.H., Miralda-Escudé J., 1996, ApJ, 457, L51

Lake G., 1988, ApJ, 327, 99

Lanzetta K.M., Bowen D.V., Tytler D. and Webb J.K., 1995, ApJ, 442, 538

Miralda-Escudé J., Rees M.J., 1993, MNRAS, 260, 624

Mo H.J., 1994, MNRAS, 269, L49

Møller P., Warren S.J., 1995, in *Galaxies in the Young Universe*, eds. Hippelein, Meisenheimer & Roeser, p88

Morris S.L., Weymann R.J., Foltz C.B., Turnshek D.A., Shectman S., Price C., Boroson T.A. 1986, ApJ, 310, 40

Navarro J.F., Frenk C.S., White S.D.M., 1995, MNRAS, 275, 56

Petitjean P., Mücket J.P., Kates R.E., 1995, A&A, 295, L9

Pettini M., Hunstead R.W., Murdoch H.S., Blades J.C. 1983, ApJ, 273, 436

Sargent W.L.W., Boksenberg A., Steidel C.C., 1988, ApJS, 68, 539

Steidel C.C., 1990, ApJS, 74, 37

Steidel C.C., 1995, in *QSO Absorption Lines*, Proc. ESO Workshop, ed. G.Meylan (Heidelberg: Springer), p. 139.

Steinmetz M., 1996, MNRAS, 278, 1005

Tytler D., Fan X.-M., Burles S., Cottrell L., Davis C., Kirkman D., Zuo L., 1995, in *QSO Absorption Lines*, Proc. ESO Workshop, ed. G.Meylan (Heidelberg: Springer), p. 289.

Vedel H., Hellsten U., Sommer–Larsen J., 1994, MNRAS, 271, 743

Warren, S. J. and Møller, P. (1995) In *New Light on Galaxy Evolution*, IAU Symposium 171, Heidelberg June 1995, in press

Wolfe A.M., 1995, in *QSO Absorption Lines*, Proc. ESO Workshop, ed. G.Meylan (Heidelberg: Springer), p. 13.

York, D.G., 1998, in *QSO Absorption Line: Probing the Universe*, Proc. of the QSO ABsorption Line Meeting, Baltimore, 1987, Cambridge University Press

Figure captions

Figure 1: The solid curves in the upper panel show the column density ratio CIV/HI as function of density for [C/H] $= -2$, a UV background with $J_{-21} = 0.3$ and spectral index $\alpha = 1.5$ beyond the Lyman edge. Calculations were done with CLOUDY for fixed temperatures. For the dashed curve the temperature is determined by photoionization equilibrium. The dotted curves are for an extremely soft spectrum with $\alpha = 5$. The lower panel shows a typical temperature/density distribution for the gas particles in our SPH simulations. The solid curves show the corresponding relation assuming photoionization equilibrium.

Figure 2: CIV and HI absorption for a mosaic of lines-of-sight around a filamentary structure at $z = 3$. HI and CIV absorption are shifted relative to each other by 0.5. Only the $\lambda1548$ line of the CIV doublet is shown. The proper distance between neighbouring panels is 10 kpc.

Figure 3: The top panels show CIV and HI absorption along selected lines-of-sight at $z = 3$. The signal-to-noise is 50, the instrumental broadening $8\,\mathrm{km\,s^{-1}}$, and the bin size $2\,\mathrm{km\,s^{-1}}$. Only the $\lambda1548$ line of the CIV doublet is shown. The next three panels show from top to bottom the corresponding total gas density, HI (solid curve) and CIV (dashed curve) weighted temperatures and the peculiar velocity profile. The bottom panels show contour plots of the CIV density in a plane containing the LOS. The spacing of the contours is 2 dex.

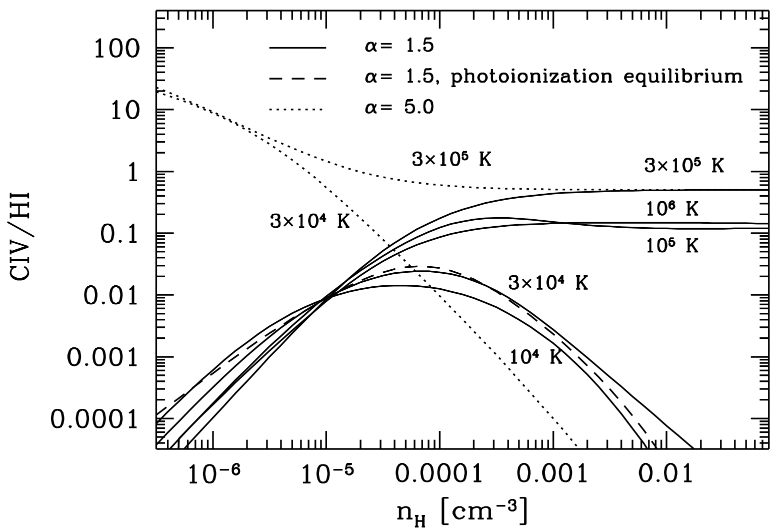

Figure 1a

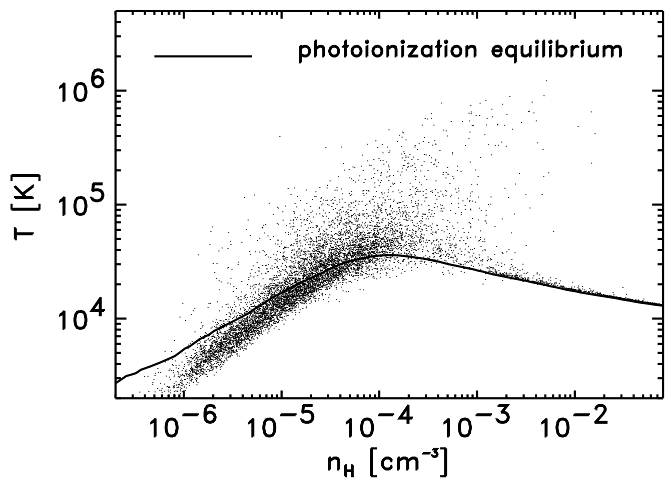

Figure 1b

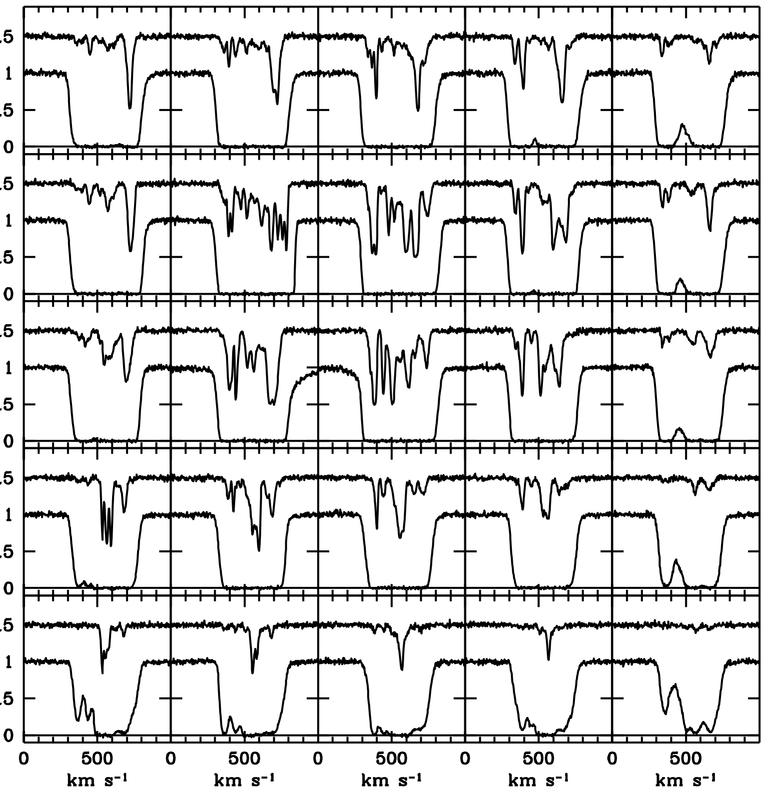

Figure 2

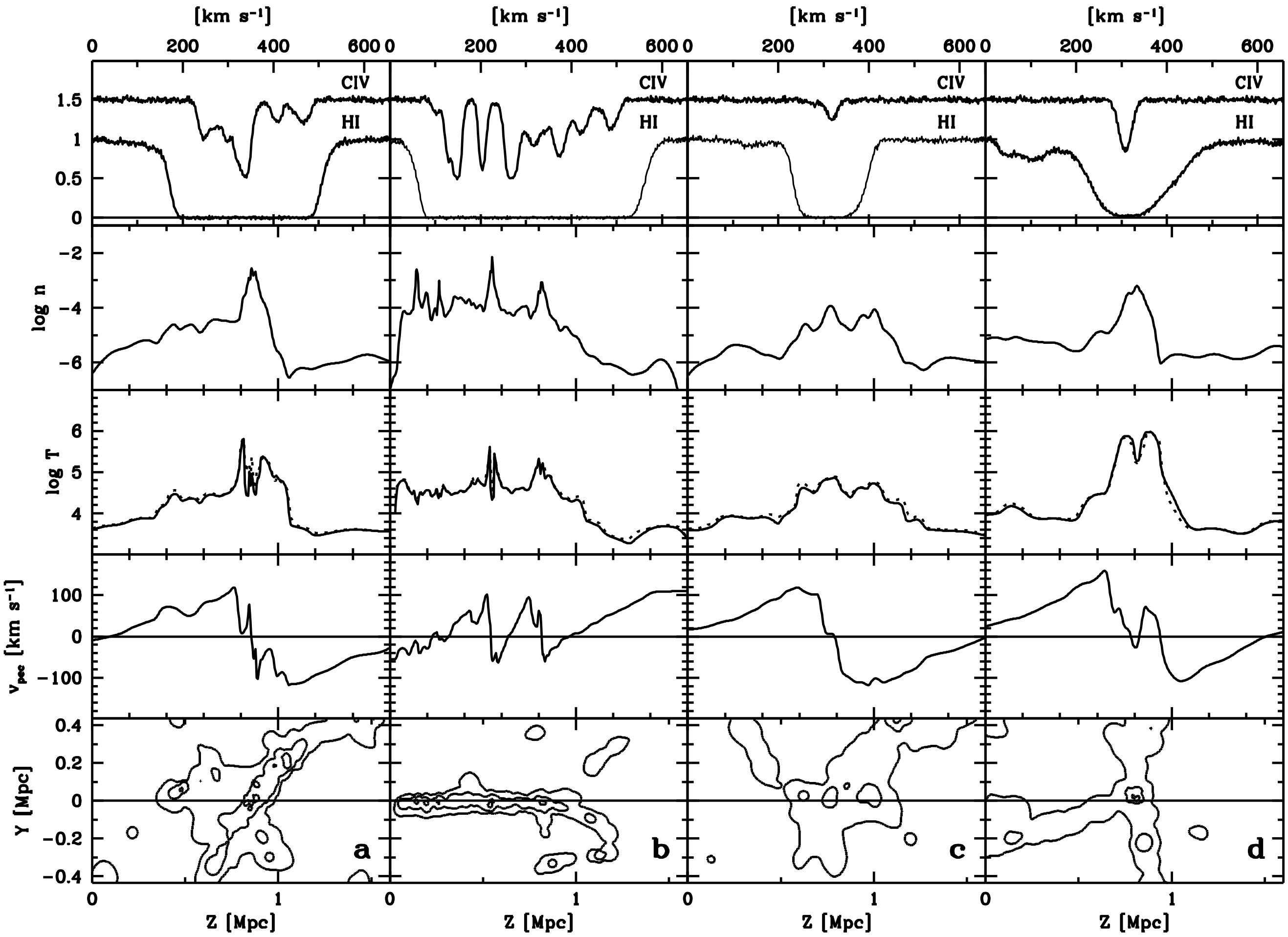

[km s-1]
0
200
400
600
CIV
HI
1.5
1
0.5
0
log n
-2
-4
-6
log T
6
5
4
v_{pec} [km s-1]
100
0
-100
Y [Mpc]
0.4
0.2
0
-0.2
-0.4
a
b
c
d
Z [Mpc]
1

Figure 3